ARTICLE

Translational and Rotational Dynamics of Individual Single-Walled Carbon Nanotubes in Aqueous Suspension

Dmitri A. Tsyboulski, Sergei M. Bachilo, Anatoly B. Kolomeisky, and R. Bruce Weisman*

Department of Chemistry, Richard E. Smalley Institute for Nanoscale Science and Technology, and Center for Biological and Environmental Nanotechnology, Rice University, 6100 Main Street, Houston, Texas 77005

ABSTRACT Near-infrared fluorescence videomicroscopy has been used to study simultaneously the translational and rotational diffusion of individual semiconducting single-walled carbon nanotubes (SWCNTs) in aqueous suspension. Analysis of translational trajectories revealed diffusion coefficient values from approximately 0.3 to 6 $\mu m^2/s$. The nanotube lengths deduced from these values ranged between ~130 nm and 6 μm. From the minor bending motions observed in individual nanotubes several micrometers in length, we confirmed that the shorter SWCNTs of primary interest here can be considered to be rigid rods under normal conditions. Because the nanotubes act as highly rigid, photostable, steady, and anisotropic fluorophores, it was possible to monitor their rotational reorientations through fluctuations in emission intensity under linearly polarized excitation. The magnitudes of observed orientational fluctuations varied substantially among individual nanotubes. These magnitudes correlated strongly with translational diffusion coefficient, reflecting the length dependence of both types of motions. Combined translational and rotational measurements also revealed the influence of local environment on nanotube mobility.

KEYWORDS: single-walled carbon nanotubes · SWCNT · fluorescence microscopy · single-nanotube imaging · diffusion · rotation · Brownian motion

Single-walled carbon nanotubes (SWCNTs) have recently been recognized as exceptional near-infrared fluorophores that possess very high photostability,[1,2] an absence of emission intermittency,[1,3] strong optical anisotropy,[4] and photoluminescence action cross sections large enough to permit individual nanotube motions to be observed using fluorescence videomicroscopy.[5−7] This combination of optical properties cannot be found in other fluorescent markers such as quantum dots, quantum rods, and fluorescent dyes.[8−10] SWCNTs are therefore uniquely promising fluorescent probes of local environments for potential applications in bioimaging and materials science. To support such applications, it is necessary to establish quantitative relations between optical imaging data and the translational and rotational motions of SWCNTs in liquids. In this report we describe the experimental methods and data analysis procedures that reveal SWCNT motional dynamics.

SWCNT samples generally contain a variety of structural species, each indexed by a pair of integers (*n*,*m*), that differ in diameter and chiral angle. Most of these species are semiconducting and display characteristic near-IR emission from excitons following the absorption of visible light. Under ambient conditions, the emission from a single SWCNT typically shows a line width of ~15−20 meV and a peak wavelength between 900 and 1600 nm reflecting its (*n*,*m*) identity.[11,12] The photostability of SWCNTs appears to be superior to that of quantum dots,[8] although these limits have not yet been fully tested.[1−3,13] Single-nanotube fluorescence studies are aided by the relatively short exciton lifetime of ~100 ps,[14−16] which allows rapid ground-state repopulation and therefore a high saturation limit for emission.[2] For SWCNTs in aqueous sodium dodecyl benzenesulfonate suspension excited on resonance with their second van Hove absorption peaks, emission increases linearly with excitation intensity for levels up to ~1−2 kW/cm^2.[6] SWCNT absorption and emission are both highly anisotropic, with reported experimental absorption and fluorescence anisotropy values (defined as $(I_{\parallel} - I_{\perp})/(I_{\parallel} + 2I_{\perp})$) reaching 0.9.[1,4,7] Recently, however, Lefebvre and Finnie demonstrated that SWCNT optical anisotropies vary somewhat with wavelength because of weak spectroscopic absorption bands with transition moments perpendicular to the nanotube axis.[17] The dominant visible absorption bands of SWCNTs have large cross sections (~1.6×10^6 cm^2 per mole of carbon atoms)[6,18,19] and give significant near-IR emission with quantum yields up to ~10% for selected SWCNT structures.[5,6] Thus, individual nano-

See the accompanying Perspective by Strano and Jin on p 1749.

*Address correspondence to weisman@rice.edu.

Received for review June 12, 2008 and accepted July 10, 2008.

Published online July 29, 2008.
10.1021/nn800364r CCC: $40.75

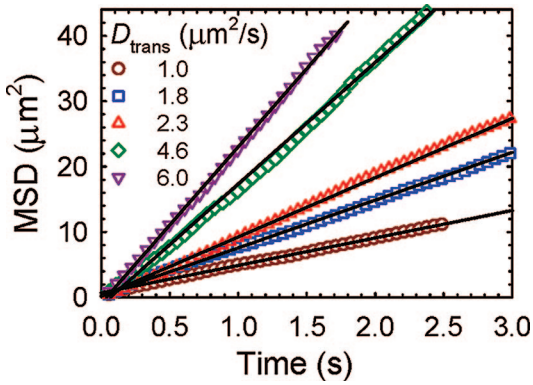

Figure 1. Mean-squared displacement graphs computed from trajectories of five individual SWCNTs and the corresponding linear fits. Only linear portions are shown. The slope of each fit equals $4D_{trans}$ for that nanotube.

tubes can easily be observed in fluores-cence microscopy using appropriate near-IR imagers and millisecond-scale exposures, as demonstrated in our earlier report.[7]

RESULTS AND DISCUSSION

Translational Diffusion of SWCNTs. SWCNTs in micelles can be modeled as rigid cylinders with large aspect ratios, for which the diffusional behavior is well-known.[20−23] Since SWCNT motions occur in three dimensions while we observe only a two-dimensional projection, the measured translational diffusion coefficient can be written as[21,22,24]

$$D_{trans} = \frac{k_B T}{6\pi\eta_s} \frac{2\ln(L/d) - \gamma_{||} - \gamma_{\perp}}{L} \quad (1)$$

where k_B is the Boltzmann constant, T is the sample temperature (296 K in our experiments), η_s is the solution viscosity (1.0 ± 0.1 mPa · s), $\gamma_{\perp}$ and $\gamma_{||}$ are end-correction coefficients,[24] d is the effective rod diameter (assumed equal to 5 nm), and L is the rod length. Lengths of nanotubes in our samples vary from ~100 nm to several micrometers,[25] whereas their effective diameters, including surfactant coating, are estimated to fall within the narrow range of 5 ± 2 nm.[26,27] Because of the logarithmic dependence on L/d in eq 1, this uncertainty in nanotube diameter will cause an uncertainty in D_{trans} of only ~12% for 200 nm long SWCNTs, and less for longer ones.

We recorded and analyzed the translational motions of 44 individual SWCNTs that were confined to a ~2 μm thick sample cell and excited with linearly polarized light. Although fluorescence intensities fluctuated as nanotubes rotated in and out of alignment with the excitation polarization, translational trajectories were still readily obtained from the videomicrographs. Initially, SWCNTs with optically unresolved dimensions were selected, ensuring that SWCNT lengths were no greater than our instrumental resolution of ~1 μm. Each nanotube trajectory was numerically analyzed using a standard mean-squared displacement (MSD) method to assess its translational motion.[28] Figure 1 shows typical MSD graphs for several SWCNTs. The linearity of these data indicates that the nanotubes are moving diffusively. As the slope of each linear fit equals $4D_{trans}$ for that nanotube, the translational diffusion coefficients deduced from Figure 1 range from 0.3 to 6 $\mu m^2/s$. From eq 1, it is clear that these differences in D_{trans} values reflect the variety of lengths among the observed nanotubes. The range of measured SWCNT D_{trans} values includes the reported diffusion coefficient of tobacco mosaic virus, a biological nanostructure of similar dimensions.[29] Note that nanotube motion in our sample cell is expected to be slowed significantly by the higher effective medium viscosity in confined environments, *i.e.*, wall-drag effects. Including an empirically determined wall-drag correction factor of ~1.6 (see Supporting Information),[22] we estimate that nanotube lengths in our sample fall in the range of ~130−6000 nm. These results are consistent with the observation that nanotubes having D_{trans} values below 1.2 $\mu m^2/s$ are optically resolvable in our apparatus and therefore must have lengths exceeding 1 μm. We note that more accurate determination of SWCNT lengths from translational diffusion coefficients requires additional attention to length-dependent near-wall effects and the use of a better defined hydrodynamic diameter for surfactant-coated nanotubes. Comparative measurements of D_{trans} values for equivalent, length-sorted SWCNT samples suspended in different surfactants should reveal the differences in their hydrodynamic diameters.

Stability of SWCNT Fluorescence. As noted earlier, SWCNTs can be considered photostable fluorophores in the sense that they resist photobleaching over long periods and are generally free from fluorescence intermittency. Prior reports demonstrated remarkably stable emission signals from individual SWCNTs in solid media,[1,2,30] and our observations find similar emission stability for SWCNTs in a liquid environment. Although the majority of individual SWCNTs in our samples are mobile, we observed a small fraction of immobilized nanotubes that appeared to be trapped at a liquid/glass interface. These are convenient subjects for measuring emission stability in the fluid environment without the complications caused by nanotube motions. Images and emission histories of such trapped nanotubes are shown in Figure 2 at different time resolutions. Figure 2A shows that emission intensities of single SWCNTs can be measured in our apparatus with high signal-to-noise ratios (~30). The nanotube shown in Figure 2B is 2.5 ± 0.5 μm long and can be imaged even with exposure times as short as 1 ms. Its emission signal recorded over 10 ms integration intervals shows only slight fluctuations, which may reflect occasional sidewall redox processes.[3] The unsurpassed emission stability and strong optical anisotropy of SWCNTs enable the follow-

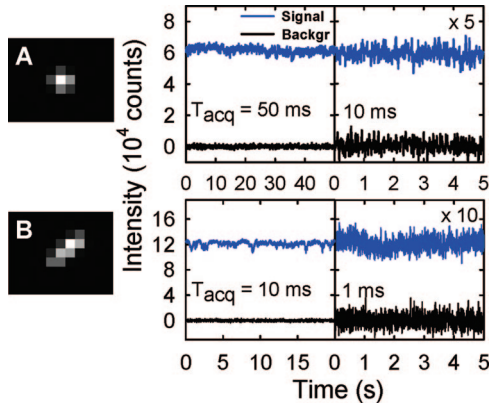

Figure 2. Near-IR fluorescence images and spatially integrated signal intensity traces for two immobilized SWCNTs recorded with acquisition intervals of 50, 10, and 1 ms. In each graph, the upper trace shows emission data from the nanotube and the lower trace shows equivalent data from a background region. Samples were excited with linearly polarized light (excitation intensity ~2 kW/cm^2). Each image pixel is 0.5 × 0.5 μm.

ing new approach to study rotational motions of individual nanoparticles with lengths too short to optically resolve.

Rotational Diffusion of SWCNTs. When excited with linearly polarized light, the fluorescence of mobile SWCNTs exhibits intense blinking. This emission modulation is entirely due to rotational motions, reflecting changing orientations of the nanotube axis relative to the excitation beam's polarization and the direction of observation. To quantify this behavior, we analyzed the emission intensity profiles of freely moving SWCNTs by calculating sums over the 7 × 7 pixel matrix centered on the pixel of maximum brightness. Background signals were obtained using a similar calculation on a nanotube-free region shifted by 12 pixels in either the *X* or the *Y* direction. The nanotube emission trace was corrected by subtracting the average signal from the background region and then scaling to give an average relative intensity of 0.290 (this constant is explained below). Figure 3 shows emission traces of nanotubes that display different D_{trans} coefficients. It is clear that the intensity fluctuations of slowly translating SWCNTs are large compared to fluctuations of those that translate more rapidly. This occurs because the more rapidly translating nanotubes are the shorter ones, which can rotate quickly enough to assume a wide range of orientations during the measurement integration period and give signals with greater orientational averaging. To slow down rotational motions and suppress this orientational averaging, we made similar measurements on a sample suspended in a 60% glycerin−40% water mixture that had a 10-fold higher viscosity.[31] As illustrated in Figure 3d, nanotubes in this viscous medium displayed the expected large fluctuations in emission intensity.

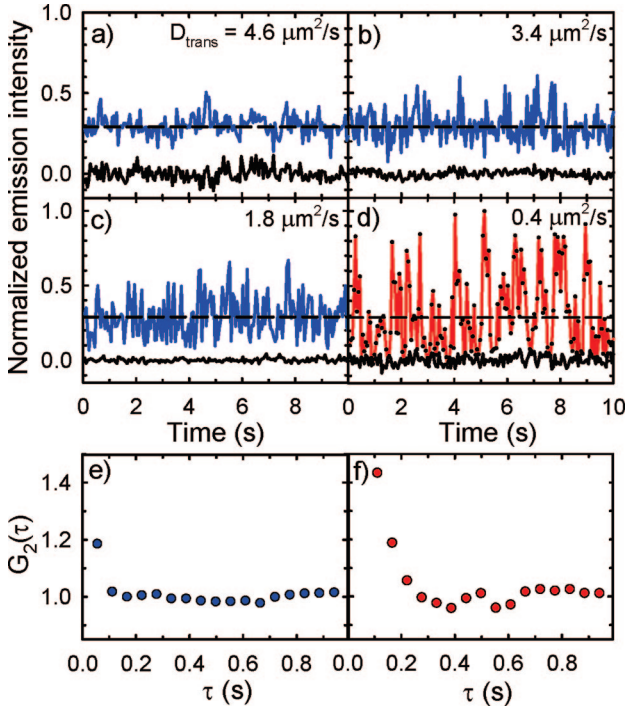

Figure 3. Fluctuating emission signals recorded with 50 ms integration times from SWCNTs with different translational diffusion coefficients. (a−c) Traces for SWCNTs in water; (d) trace for a SWCNT in a glycerin−water mixture with 10-fold higher viscosity. (e,f) Autocorrelation functions of the SWCNT emission traces in (c) and (d), respectively.

The exponential time decay in a rotational autocorrelation function is commonly used to evaluate the rotational diffusion coefficient.[32] Figure 3e,f displays the related intensity autocorrelation functions calculated from the emission traces of Figure 3c,d. The unresolved rapid decay found for SWCNT rotation in water (Figure 3e) demonstrates that our experimental time resolution is not adequate to support this approach. However, autocorrelation analysis will be more useful if SWCNT rotational speed is significantly decreased, as shown in Figure 3d,f, or if the instrumental time resolution is substantially improved. According to Broersma theory,[20,21] the rotational diffusion coefficient D_{rot} of a rigid rod is given as

$$D_{rot} = \frac{3k_BT}{\pi\eta_s}\frac{\ln(L/d) - \gamma_r}{L^3} \quad (2)$$

where γ_r is a length-dependent end-correction coefficient.[24] Using eq 2, one can estimate that nanotubes of length 500 nm will rotationally diffuse in water by an average of nearly 1000° during our 50 ms measurement interval, thereby giving fully rotationally averaged signals. In view of the inverse cubic dependence of D_{rot} on SWCNT length, it does not seem feasible to resolve the rotational motions of shorter nanotubes, even with millisecond temporal resolution.

An alternative approach is to examine the magnitudes of SWCNT emission signal fluctuations and correlate them with rotational mobility. As the nanotube randomly reorients during the measurement interval, its

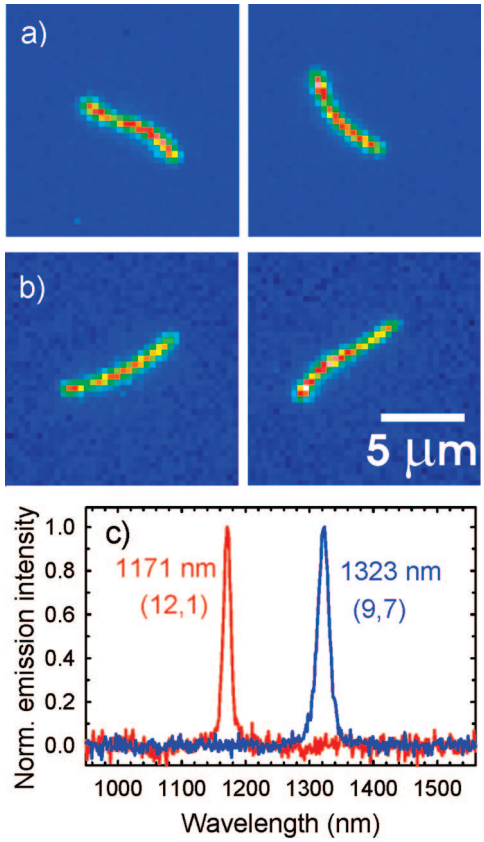

Figure 4. Bending of long individual SWCNTs in water. Selected image frames of (a) a (12,1) SWCNT, and (b) a (9,7) SWCNT recorded at 90 × magnification and false-colored. Nanotube (*n*,*m*) values were determined from their emission spectra, shown in (c).

fluorescence signal becomes averaged over a range of SWCNT orientations. Clearly, faster rotation results in greater averaging, as demonstrated in Figure 3. Furthermore, the average emission signal, $\langle I \rangle$, of any randomly rotating nanotube acquired over a sufficiently long time interval can be shown to equal a constant fraction of the maximum emission signal, I_{max}, measured when it is stationary and aligned in the polarization plane of the excitation beam and perpendicular to the observation axis. Thus, the relative SWCNT emission signal fluctuations can serve as a measure of SWCNT rotational diffusion speed.

This approach assumes that the nanotubes of interest are rigid enough to avoid optical depolarization effects caused by curvature. To check this assumption, we have optically imaged individual nanotubes that have lengths significantly above the diffraction limit. These unusually long SWCNTs were prepared from raw HiPco material using short ultrasonication times, and the resulting aqueous suspensions were then examined using near-IR fluorescence microscopy with circularly polarized excitation.[7] The diffusional motion of these long nanotubes is slow enough to allow us to capture their emission spectra and thereby deduce their (*n*,*m*) identities.[11,33] Figure 4a,b shows images of two long nanotubes, and Figure 4c shows their emission spectra. From the peak positions of 1171 and 1323 nm, these SWCNTs were identified as the (12,1) and (9,7) species.[33] We observe that these long nanotubes undergo moderate, thermally induced bending at radii of curvature down to ~5−10 μm. Therefore, the shorter SWCNTs (<1−2 μm long) that predominate in our diffusional studies have negligible bending and can properly be treated as rigid rods in the following optical analysis. We note, however, that stiffness is expected to depend on diameter,[23,34] and further studies to quantify SWCNT bending stiffness as a function of structure are in progress.

Combined Rotational and Translational Analysis. Because of the high stiffness and strong optical anisotropy of SWCNTs, their absorption and emission can be described using a dipole oscillator model with transition moment aligned along the tube axis. Defining the common axis of excitation and observation as *Z*, the instantaneous emission signal for excitation polarized in the *XZ* plane and unpolarized detection is proportional to $\sin^4 \alpha \cos^2 \varphi$. Here, $\alpha \in [0,\pi]$ and $\varphi \in [0, 2\pi]$ are spherical polar coordinates that define the azimuthal and equatorial angles of the SWCNT orientation with respect to the *Z* axis. It is easily shown that $\langle I \rangle / I_{max} = \langle \sin^4 \alpha \cos^2 \varphi \rangle = 0.267$. However, if the observation is expanded to a cone representing high numerical aperture collection optics, $\langle I \rangle / I_{max}$ changes to 0.290 or 0.311 for NA values of 1.0 and 1.4, respectively (see Supporting Information).

To model the variations in emission intensity induced by nanotube rotational diffusion, we performed "random walk on a unit sphere" numerical simulations. A detailed description of this procedure is provided in the Supporting Information. We computed simulated time-resolved emission intensity profiles for SWCNTs with lengths between 100 and 10000 nm whose rotation is described by eq 2. These simulated profiles were in excellent qualitative agreement with experimental data. For a quantitative comparison, we computed the standard deviations σ of simulated and experimental emission traces. Because emission data are measured against a noisy background, we corrected the raw standard deviations of experimental intensity signals using the relation $\sigma = (\sigma^2_{raw} - \sigma^2_{bkgd})^{1/2}$, where σ_{bkgd} is the standard deviation of the background trace. (Shot noise is not dominant in our measurements.) Figure 5 shows these corrected experimental fluctuation values plotted against the translational diffusion coefficients measured for the same nanotubes. Also plotted are lines displaying theoretical results computed using several models. The dotted line ("model 1") shows σ values found from numerical simulations of idealized SWCNT rotational diffusion plotted against translational diffusion coefficients found from eq 1.

The data clearly display the tendency of σ to increase as D_{trans} decreases, as expected from the length-dependent behaviors discussed above. The systematic deviations between model and experiment seen in Fig-

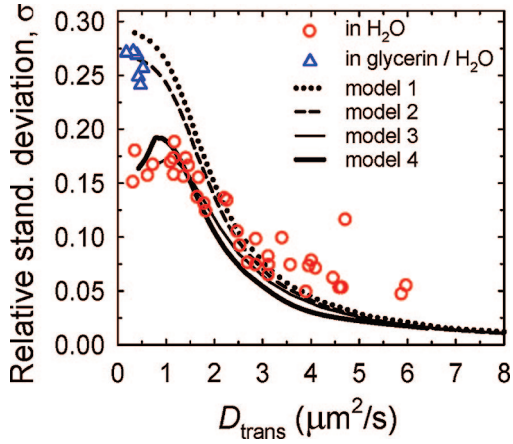

Figure 5. Theoretical and experimental standard deviations σ of SWCNT emission signals plotted against the corresponding translational diffusion coefficients. The dotted (model 1) curve is computed according to Broersma theory (eqs 1 and 2) for the data acquisition conditions described in the text. The other curves show results for adjusted models as discussed in the text. Red circles and blue triangles represent data measured for SWCNTs in water and a water−glycerin mixture (with ~10-fold higher viscosity), respectively.

ure 5 are predominantly caused by several effects that change the value of $\langle I \rangle / I_{max}$. The first effect concerns the optical anisotropy of SWCNTs, which we assumed to be ideal in our initial treatment. In fact, however, SWCNT absorption anisotropy may vary from 0.9 to 0.6, depending on how closely the excitation wavelength matches the SWCNT E_{22} spectral peak.[4,17] As our measurements were made mainly on the brightest nanotubes, which had E_{22} peaks near the excitation wavelength, we estimate an average absorption anisotropy value of ~0.86 ($I_\perp / I_\parallel = 0.05$). This adjustment raises the normalization parameter $\langle I \rangle / I_{max}$ from 0.290 to 0.315 (for a detection NA of 1.0), thereby reducing σ by the factor 0.290/0.315 or 0.92 (see Supporting Information). The dashed line labeled "model 2" in Figure 5 includes this adjustment for non-ideal absorption anisotropy.

Another effect to include is the constrained rotation of longer nanotubes in our thin sample cell. Whereas SWCNTs much shorter than the cell thickness can rotate without cell constraints in three dimensions, longer ones rotate preferentially in the plane normal to the observation axis. This effect causes a length-dependent increase in the normalization parameter, to a limiting value of 0.5 for nanotubes much longer than the cell thickness. Expected σ values are thereby reduced, particularly for long (small D_{trans}) SWCNTs (see Supporting Information for details). The curve labeled "model 3" in Figure 5 shows the "model 2" results adjusted to include this constrained rotation correction.

Finally, it is also important to correct for the wall-drag effect that is known to impede the motions of particles in confined geometries.[22,35] This effect is usually taken into account through an increased effective viscosity. For "rigid rod" actin filaments, Li and Tang found empirical near-wall effective viscosities 1.9 ± 0.3 and 3.0 ± 1.8 times higher than bulk values for translational and rotational diffusion, respectively.[22] By analyzing the trajectories of SWCNTs that are long enough to measure their lengths from optical images, we similarly find translational diffusion coefficients that are approximately a factor of 1.6 lower than predicted using eq 1 with bulk viscosity values (see Supporting Information). The "model 4" curve in Figure 5 shows the "model 3" prediction after adjustment to include increased effective viscosities for translational ($1.6\eta_s$) and rotational ($2.5\eta_s$) diffusion of all nanotubes.

The triangular symbols in Figure 5 represent data measured for SWCNTs that are predominately less than 500 nm long[25] and are suspended in a glycerin−water solution. This medium is viscous enough to greatly slow the nanotube motions and allow full resolution of their rotationally induced emission fluctuations, while the nanotubes are short enough to avoid orientational constraints from the cell walls. The σ values measured for these nanotubes reach approximately 0.27, in agreement with model 2. This confirms our estimate of the SWCNT average anisotropy. The open circles in Figure 5 show data measured for SWCNTs in normal water. These points represent a wide range of nanotube lengths and could be influenced by all of the effects incorporated into model 4, which in fact fits the data quite well without adjustable parameters. Models 3 and 4 successfully mimic the experimental "kink" seen near $D_{trans} = 1\ \mu m^2/s$, where the SWCNT length becomes comparable to the sample cell thickness. For faster moving nanotubes (with larger D_{trans} values), model 4 systematically underestimates σ. This may reflect an experimental artifact caused by extra relative noise in the weaker emission signals from short nanotubes, or it may arise because short nanotubes experience reduced wall-drag. Further analysis of length-sorted SWCNT samples[36−39] will help to clarify this point. The simultaneous measurement of σ and D_{trans} for individual SWCNTs provides new information about the motional constraints imposed on nanoparticles by their local environment.

SUMMARY

We have exploited the remarkably high photostability, mechanical rigidity, and optical anisotropy of SWCNTs to make fluorescence-based measurements of single-nanoparticle translational diffusion in fluid media. This analysis allows the lengths of individual nanotubes to be deduced from their mobilities, even for nanotubes too short to resolve by optical imaging. Our techniques will allow detailed studies of optical properties, such as photoluminescence action cross sections, as a function of nanotube length. Careful measurements of translational diffusion coefficients should also reveal the differences in hydrodynamic coating thickness among various nano-

tube surfactants. In addition, we have presented a novel method for deducing the orientational mobility of individual SWCNTs from fluctuations in their emission intensities. Combined measurements that reveal restrictions in nanotube translational and rotational motions can give valuable insights into the geometry of constrained environments such as thin liquid layers, nanoscale pores, and intracellular structures.

METHODS

Sample Preparation Procedures. Our samples were prepared from aqueous suspensions of raw HiPco SWCNTs in 1% sodium dodecyl benzenesulfonate at pH 8 using procedures reported previously.[26] After dilution to SWCNT concentrations near 1 ng/mL, 1.3 μL portions were spread between a quartz microscope slide and a coverslip to yield aqueous films ~2.0 ± 0.5 μm thick. This film thickness allows continuous observation of SWCNTs because it matches the optical depth-of-field of our microscope's water-immersion objective lens. The edges of the sample chamber were sealed to prevent liquid evaporation and convection.

Near-IR Videomicroscopy and Spectroscopy of Individual SWCNTS. Nanotube motions in the aqueous suspensions were recorded using a custom experimental setup that was described earlier.[7] In brief, a Nikon TE-2000U inverted microscope was equipped with Nikon PlanApo 60×/1.0 NA water-immersion objective. A dichroic beamsplitter and a 946 nm long-pass filter selected emission in the desired near-IR wavelength range. An InGaAs near-IR imager (OMA-V 2D, Roper Scientific) was installed on one output port of the microscope. At another port, the image plane was coupled *via* a fiber-optic cable (100 μm core diameter) to the entrance slit of a J-Y C140 spectrograph with a 512-element InGaAs detector array (OMA-V, Roper Scientific) mounted in its focal plane. Emission spectra between 950 and 1580 nm were thereby acquired from selected spatial regions measuring ~1.5 μm in diameter at the sample for 60× magnification. Samples were excited from above with an external 785 nm diode laser (power at the sample ~40 mW). An aspheric lens (f = 18.4 mm) mounted on an *XYZ* translation stage focused the excitation beam to a spot of ~60 μm in diameter. The maximum excitation intensity at the sample was approximately 1.5 kW/cm.^{2} The excitation polarization was purified with a crystalline Glan polarizer and then controlled with λ/4 and λ/2 retardation plates. Linear polarization purity was ≥0.99, while circular polarization ellipticity was ≥0.95. To reduce the imager readout time to ~5 ms, only a small region of interest, 30 × 30 μm containing 3600 pixels, was used to record SWCNT motion. At least 350 consecutive frames were acquired during each measurement sequence using frame acquisition times of 50 ms.

Computational Methods. Numerical simulations of SWCNT rotational motion were performed using a custom procedure described in section B of the Supporting Information. Integral expressions were evaluated numerically using the Mathcad 2001 computational package.

Acknowledgment. We thank M. Pasquali, L. Cognet, and D. Budhadipta for helpful discussions and experimental assistance. This research was funded by the Welch Foundation (grant C-0807 to R.B.W., grant C-1559 to A.B.K., and postdoctoral fellowship L-C-0004 to D.A.T.), the NSF Center for Biological and Environmental Nanotechnology (grant EEC-0647452), and Applied NanoFluorescence, LLC.

Supporting Information Available: Analytical expressions describing the dependence of SWCNT emission intensity on spatial orientation; algorithm for numerical simulation of nanotube rotational dynamics; correction factors affecting the ratio $\langle I \rangle / I_{max}$; and experimental results showing the influence of wall-drag effects on SWCNT mobility. This material is available free of charge *via* the Internet at http://pubs.acs.org.

REFERENCES AND NOTES

1. Hartschuh, A.; Pedrosa, H. N.; Novotny, L.; Krauss, T. D. Simultaneous Fluorescence and Raman Scattering from Single Carbon Nanotubes. *Science* **2003**, *301*, 1354–1356.
2. Matsuda, K.; Kanemitsu, Y.; Irie, K.; Saiki, T.; Someya, T.; Miyauchi, Y.; Maryama, S. Photoluminescence Intermittency in an Individual Single-Walled Carbon Nanotube at Room Temperature. *Appl. Phys. Lett.* **2005**, *86*, 12316-1–12316-3.
3. Cognet, L.; Tsyboulski, D.; Rocha, J.-D. R.; Doyle, C. D.; Tour, J. M.; Weisman, R. B. Stepwise Quenching of Exciton Fluorescence in Carbon Nanotubes by Single-Molecule Reactions. *Science* **2007**, *316*, 1465–1468.
4. Lefebvre, J.; Fraser, J. M.; Finnie, P.; Homma, Y. Photoluminescence from an Individual Single-Walled Carbon Nanotube. *Phys. Rev. B* **2004**, *69*, 075403-1–075403-5.
5. Lefebvre, J.; Austing, D. G.; Bond, J.; Finnie, P. Photoluminescence Imaging of Suspended Single-Walled Carbon Nanotubes. *Nano Lett.* **2006**, *6*, 1603–1608.
6. Tsyboulski, D.; Rocha, J.-D. R.; Bachilo, S. M.; Cognet, L.; Weisman, R. B. Structure-Dependent Fluorescence Efficiencies of Individual Single-Walled Carbon Nanotubes. *Nano Lett.* **2007**, *7*, 3080–3085.
7. Tsyboulski, D. A.; Bachilo, S. M.; Weisman, R. B. Versatile Visualization of Individual Single-Walled Carbon Nanotubes with Near-Infrared Fluorescence Microscopy. *Nano Lett.* **2005**, *5*, 975–979.
8. van Sark, W. G. J. H. M.; Frederix, P. L. T. M.; Bol, A. A.; Gerritsen, H. C.; Meijerink, A. Blueing, Bleaching, and Blinking of Single CdSe/ZnS Quantum Dots. *ChemPhysChem* **2002**, *3*, 871–879.
9. Zondervan, R.; Kulzer, F.; Orlinskii, S. B.; Orrit, M. Photoblinking of Rhodamine 6G in Poly(vinyl alcohol): Radical Dark State Formed through the Triplet. *J. Phys. Chem. A* **2003**, *107*, 6770–6776.
10. Tsay, J. M.; Doose, S.; Weiss, S. Rotational and Translational Diffusion of Peptide-Coated CdSe/CdS/ZnS Nanorods Studied by Fluorescence Correlation Spectroscopy. *J. Am. Chem. Soc.* **2006**, *128*, 1639–1647.
11. Bachilo, S. M.; Strano, M. S.; Kittrell, C.; Hauge, R. H.; Smalley, R. E.; Weisman, R. B. Structure-Assigned Optical Spectra of Single-Walled Carbon Nanotubes. *Science* **2002**, *298*, 2361–2366.
12. Wang, F.; Dukovic, G.; Brus, L. E.; Heinz, T. F. The Optical Resonances in Carbon Nanotubes Arise from Excitons. *Science* **2005**, *308*, 838–841.
13. Heller, D. A.; Baik, S.; Eurell, T. E.; Strano, M. S. Single-Walled Carbon Nanotube Spectroscopy in Live Cells: Towards Long-Term Labels and Optical Sensors. *Adv. Mater.* **2005**, *17*, 2793–2799.
14. Hagen, A.; Steiner, M.; Raschke, M. B.; Lienau, C.; Hertel, T.; Qian, H.; Meixner, A. J.; Hartschuh, A. Exponential Decay Lifetimes of Excitons in Individual Single-Walled Carbon Nanotubes. *Phys. Rev. Lett.* **2005**, *95*, 197401-1–197401-4.
15. Jones, M.; Engtrakul, C.; Metzger, W. K.; Ellingson, R. J.; Nozik, A. J.; Heben, M. J.; Rumbles, G. Analysis of Photoluminescence from Solubilized Single-Walled Carbon Nanotubes. *Phys. Rev. B* **2005**, *71*, 115426-1–115426-9.
16. Jones, M.; Metzger, W. K.; McDonald, T. J.; Engtrakul, C.; Ellingson, R. J.; Rumbles, G.; Heben, M. J. Extrinsic and Intrinsic Effects on the Excited-State Kinetics of Single-Walled Carbon Nanotubes. *Nano Lett.* **2007**, *7*, 300–306.
17. Lefebvre, J.; Finnie, P. Polarized Photoluminescence Excitation Spectroscopy of Single-Walled Carbon Nanotubes. *Phys. Rev. Lett.* **2007**, *98*, 167406-1–167406-4.

18. Islam, M. F.; Milkie, D. E.; Kane, C. L.; Yodh, A. G.; Kikkawa, J. M. Direct Measurement of the Polarized Optical Absorption Cross Section of Single-Wall Carbon Nanotubes. *Phys. Rev. Lett.* **2004**, *93*, 037404-1–037404-4.
19. Fagan, J. A.; Simpson, J. R.; Landi, B. J.; Richter, L. J.; Mandelbaum, I.; Bajpai, V.; Ho, D. L.; Raffaelle, R.; Hight Walker, A. R.; Bauer, B. J.; et al. Dielectric Response of Aligned Semiconducting Single-Wall Nanotubes. *Phys. Rev. Lett.* **2007**, *98*, 147402-1–147402-4.
20. Broersma, S. Rotational Diffusion Constant of a Cylindrical Particle. *J. Chem. Phys.* **1960**, *32*, 1626–1631.
21. Broersma, S. Viscous Force Constant for a Closed Cylinder. *J. Chem. Phys.* **1960**, *32*, 1632–1635.
22. Li, G.; Tang, J. X. Diffusion of Actin Filaments within a Thin Layer Between Two Walls. *Phys. Rev. E.* **2004**, *69*, 061921-1–061921-5.
23. Duggal, R.; Pasquali, M. Dynamics of Individual Single-Walled Carbon Nanotubes in Water by Real-Time Visualization. *Phys. Rev. Lett.* **2006**, *96*, 246104-1–246104-4.
24. Broersma, S. Viscous Force and Torque Constants for a Cylinder. *J. Chem. Phys.* **1981**, *74*, 6989–6990.
25. Ziegler, K. J.; Rauwald, U.; Gu, Z. N.; Liang, F.; Billups, W. E.; Hauge, R. H.; Smalley, R. E. Statistically Accurate Length Measurements of Single-Walled Carbon Nanotubes. *J. Nanosci. Nanotechnol.* **2007**, *7*, 2917–2921.
26. O'Connell, M.; Bachilo, S. M.; Huffman, C. B.; Moore, V.; Strano, M. S.; Haroz, E.; Rialon, K.; Boul, P. J.; Noon, W. H.; Kittrell, C.; et al. Band-Gap Fluorescence from Individual Single-Walled Carbon Nanotubes. *Science* **2002**, *297*, 593–596.
27. Richard, C.; Balavoine, F.; Schultz, P.; Ebbesen, T. W.; Mioskowski, C. Supramolecular Self-Assembly of Lipid Derivatives on Carbon Nanotubes. *Science* **2003**, *300*, 775–778.
28. Rieger, B.; Dietrich, H. R. C.; van den Doel, L. R.; van Vliet, L. J. Diffusion of Microspheres in Sealed and Open Microarrays. *Microsc. Res. Tech.* **2004**, *65*, 218–225.
29. King, T. A.; Knox, A.; McAdam, J. D. G. Translational and Rotational Diffusion of Tobacco Mosaic Virus from Polarized and Depolarized Light Scattering. *Biopolymers* **1973**, *12*, 1917–1926.
30. Hartschuh, A.; Pedrosa, H. N.; Peterson, J.; Huang, L.; Anger, P.; Qian, H.; Meixner, A.; Steinert, M.; Novotny, L.; Krauss, T. D. Single Carbon Nanotube Optical Spectroscopy. *ChemPhysChem* **2005**, *6*, 577–582.
31. Wheast, R. C., Astle, M. J., Eds. *CRC Handbook of Chemistry and Physics*, 61 ed.; CRC Press, Inc.: Boca Raton, FL, 1981.
32. Doi, M.; Edwards, S. F. *The Theory of Polymer Dynamics*; Oxford University Press: New York, 1986.
33. Weisman, R. B.; Bachilo, S. M. Dependence of Optical Transition Energies on Structure for Single-Walled Carbon Nanotubes in Aqueous Suspension: An Empirical Kataura Plot. *Nano Lett.* **2003**, *3*, 1235–1238.
34. Ru, C. Q. Effective Bending Stiffness of Carbon Nanotubes. *Phys. Rev. B* **2000**, *62*, 9973–9976.
35. Lin, B.; Yu, J.; Rice, S. A. Direct Measurements of Constrained Brownian Motion of an Isolated Sphere Between Two Walls. *Phys. Rev. E* **2000**, *62*, 3909–3919.
36. Farkas, E.; Anderson, M. E.; Chen, Z. H.; Rinzler, A. G. Length Sorting Cut Single Wall Carbon Nanotubes by High Performance Liquid Chromatography. *Chem. Phys. Lett.* **2002**, *363*, 111–116.
37. Huang, X.; Mclean, R. S.; Zheng, M. High-Resolution Length Sorting and Purification of DNA-Wrapped Carbon Nanotubes by Size-Exclusion Chromatography. *Anal. Chem.* **2005**, *77*, 6225–6228.
38. Chun, J.; Fagan, J. A.; Hobbie, E. K.; Bauer, B. J. Size Separation of Single-Wall Carbon Nanotubes by Flow-Field Flow Fractionation. *Anal. Chem.* **2008**, *80*, 2514–2523.
39. Fagan, J. A.; Becker, M. L.; Chun, J.; Hobbie, E. K. Length Fractionation of Carbon Nanotubes Using Centrifugation. *Adv. Mater.* **2008**, *20*, 1609–1613.